10.0 Vadose Zone Remediation, Monitoring, and Characterization

D. C. Weekes and R. Khaleel

Vadose zone monitoring using leachate and soil gas sampling occurred at three areas on the Hanford Site in calendar year (CY) 2009. Leachate and soil vapor monitoring continued at the Environmental Restoration Disposal Facility (ERDF) and the Solid Waste Landfill. Monitoring for the ERDF is discussed in Section 6.5.4 and for the Solid Waste Landfill in Section 5.4.7. Soil vapor monitoring at the carbon tetrachloride expedited response action site also continued during CY 2009.

The Tank Farm Vadose Zone Project installed direct-push boreholes at the C and TY Tank Farms for subsurface characterization of unplanned releases and future geophysical surveys. The Tank Farm Vadose Zone Project also completed surface geophysical exploration at Waste Management Areas (WMAs) TX-TY and S-SX to map subsurface contaminant distribution. An interim surface barrier was placed over tank 241-T-106 to reduce the infiltration of water into the area of contamination resulting from the 1973 leak from that tank. The monitoring and characterization efforts are summarized in this chapter.

Final interpretation of data collected at the Sisson and Lu vadose zone field injection test site in the 200 East Area from the year 2000 is presented in this chapter. The concept discussed is that of upscaling, which uses small, core-scale measurements of hydraulic properties to model the large, field-scale behavior. An application of the upscaled model to data collected at the Sisson and Lu field injection site suggests that the model provides an accurate simulation of moisture flow in the heterogeneous vadose zone. The heterogeneous media at the injection site is composed of multiple strata, each of which is represented in the upscaled model by an anisotropic equivalent homogeneous medium. When the flow domain was modeled as being mildly anisotropic with the upscaled parameters, the simulated plume matched best the center of mass and the spread of the injected water of the observed moisture plume.

Information in this chapter covers the period from October 1, 2008, through December 31, 2009. The following date conventions are used throughout this report:

- Fiscal year (FY) 2009: Refers to the fiscal year named (i.e., October 1, 2008, to September 30, 2009).
- Calendar year (CY) 2009: Refers to the calendar year named (i.e., January 1, 2009, to December 31, 2009).
- Reporting period: Refers to the entire 15-month reporting period covered in this report (i.e., October 1, 2008, to December 31, 2009).

10.1 Carbon Tetrachloride Soil Vapor Monitoring and Remediation

V. J. Rohay

Soil vapor extraction is used to remove carbon tetrachloride from the vadose zone in the 200 West Area. The U.S. Environmental Protection Agency and the Washington State Department of Ecology authorized the U.S. Department of Energy to initiate this remediation in 1992 as a *Comprehensive Environmental Response, Compensation, and Liability Act of 1980* (CERCLA) expedited response action.

This section summarizes the FY 2009 activities associated with carbon tetrachloride removal. A report containing the detailed results of FY 2009 activities will be issued in CY 2010. Historic monitoring and remediation results are documented in several reports, including the following:

- BHI-00720, *Performance Evaluation Report for Soil Vapor Extraction Operations at the Carbon Tetrachloride Site, February 1992-September 2001*
- SGW-33746, *Performance Evaluation Report for Soil Vapor Extraction Operations at the 200-PW-1 Operable Unit Carbon Tetrachloride Site, Fiscal Year 2006*
- SGW-37111, *Performance Evaluation Report for Soil Vapor Extraction Operations at the 200-PW-1 Operable Unit Carbon Tetrachloride Site, Fiscal Year 2007*
- SGW-40456, *Performance Evaluation Report for Soil Vapor Extraction Operations at the 200-PW-1 Carbon Tetrachloride Site, Fiscal Year 2008*
- WMP-17869, *Performance Evaluation Report for Soil Vapor Extraction Operations at the 200-PW-1 Carbon Tetrachloride Site, Fiscal Year 2002*
- WMP-21327, *Performance Evaluation Report for Soil Vapor Extraction Operations at the 200-PW-1 Carbon Tetrachloride Site, Fiscal Year 2003*
- WMP-26178, *Performance Evaluation Report for Soil Vapor Extraction Operations at the 200-PW-1 Carbon Tetrachloride Site, Fiscal Year 2004*
- WMP-30426, *Performance Evaluation Report for Soil Vapor Extraction Operations at the 200-PW-1 Carbon Tetrachloride Site, Fiscal Year 2005*.

In FY 2009, two new soil vapor extraction systems began operating to remove carbon tetrachloride from the vadose zone. Each of the new systems has an extraction capacity of 14.2 cubic meters per minute. Figure 10-1 shows the locations of soil vapor extraction wells.

One new soil vapor extraction system was operated at the 216-Z-1A well field, and one system was operated at the 216-Z-9 well field. Each system was operated from April 1 through September 30, 2009. Temporarily suspending soil vapor extraction operations at each well field during the winter allows the carbon tetrachloride concentrations to recharge and be extracted more efficiently and economically when operations resume. Section 10.1.1 discusses the results of the FY 2009 soil vapor extraction in more detail.

To track the effectiveness of the remediation effort, soil vapor concentrations of carbon tetrachloride were monitored at the inlets to the soil vapor extraction systems and at individual online extraction wells during the 6-month operating period. To assess the impact of the soil vapor extraction system on subsurface concentrations, soil vapor concentrations of carbon tetrachloride were monitored at offline wells and probes during the entire FY (Section 10.1.2). Remediation efforts during FY 2009 also included passive soil vapor extraction (Section 10.1.3).

Approximately 79,600 kilograms of carbon tetrachloride had been removed since extraction operations started in 1991. The mass of carbon tetrachloride removed in FY 2009 was 177 kilograms.

10.1.1 Soil Vapor Extraction

During CY 2009, soil vapor extraction operations continued from April 1, 2009, through September 30, 2009, using two new, 14.2 cubic meter per minute soil vapor extraction systems. One system operated at the 216-Z-1A well field and one system operated at the 216-Z-9 well field.

For the system at the 216-Z-1A well field, initial online wells were selected within the perimeter of the 216-Z-1A Tile Field. For the system at the 216-Z-9 well field,

initial online wells were selected near the 216-Z-9 Trench. As extraction continued at both locations, additional wells in the vicinity of these two waste sites were brought online. Extraction wells open near the less-permeable Cold Creek unit, where the highest carbon tetrachloride concentrations have been detected consistently in the past, were selected at both locations to optimize mass removal of the contaminant. Extraction wells open near the groundwater were also selected for soil vapor extraction or passive soil vapor extraction (Section 10.1.3).

As of September 2009, ~79,557 kilograms of carbon tetrachloride had been removed from the vadose zone since extraction operations started in 1991 (Table 10-1). The mass of carbon tetrachloride removed in FY 2009 was 177 kilograms. The most recent performance evaluation report (SGW-40456) provides the amount of carbon tetrachloride removed per year between 1991 and 2008.

10.1.2 Monitoring of Offline Wells and Probes

During FY 2009, soil vapor concentrations of carbon tetrachloride were monitored near the ground surface, near the Cold Creek unit (~40 meters below ground surface [bgs]), and near groundwater (~66 meters bgs). Soil vapor concentrations were monitored near the ground surface and groundwater to evaluate if non-operation of the soil vapor extraction system negatively affects the soil atmosphere or groundwater. The maximum concentration detected near the ground surface (between 2 and 10 meters bgs) was 7 parts per million by volume (ppmv). Near the groundwater (between 53 and 66 meters bgs), the maximum concentration was 14 ppmv.

Soil vapor concentrations were also monitored above and within the Cold Creek unit to provide an indication of concentrations that could be expected during restart of the soil vapor extraction system. The maximum concentration detected near the Cold Creek unit (between 25 and 44 meters bgs) was 228 ppmv in soil vapor probe CPT-28 (27 meters bgs), ~90 meters south of the 216-Z-9 Trench. This location may be beyond the zone of influence of the soil vapor extraction system. Within the 216-Z-9 well field, the maximum carbon tetrachloride concentration detected near the Cold Creek unit was 50 ppmv at well 299-W15-217 (35 meters bgs). At the 216-Z-1A well field, the maximum carbon tetrachloride concentration detected near the Cold Creek unit was 186 ppmv at well 299-W18-167 (32 meters bgs).

The maximum carbon tetrachloride concentrations detected in the vadose zone overlying the Cold Creek unit (between 11 and 23 meters bgs) were 327 ppmv at well C4938 and 397 ppmv at well C4937 (both 20 meters bgs) near the 216-Z-9 Trench.

The temporary suspension of soil vapor extraction in FY 2009 appears to have caused minimal detectable vertical transport of carbon tetrachloride through the soil surface to the atmosphere. Data collected during suspension of soil vapor extraction indicate that carbon tetrachloride concentrations did not increase significantly at the near-surface monitoring probes. Carbon tetrachloride concentrations also did not increase significantly near the water table during that time, which indicates that suspending operations of the soil vapor extraction system did not negatively impact groundwater quality.

10.1.3 Passive Soil Vapor Extraction

Passive soil vapor extraction is a remediation technology that uses naturally induced pressure gradients between the subsurface and the ground surface to drive soil vapor to the surface. In general, falling atmospheric pressure causes subsurface vapor to move to the atmosphere through wells, whereas rising atmospheric pressure causes atmospheric air to move into the subsurface. Passive soil vapor extraction

systems are designed to use this phenomenon to remove carbon tetrachloride from the vadose zone.

Passive soil vapor extraction systems were installed at the end of FY 1999 at eight wells open near the vadose-groundwater interface at the 216-Z-1A/216-Z-12/216-Z-18 well field. The passive systems have check valves that allow only soil vapor flow out of the borehole (i.e., one-way movement) and canisters holding granular activated carbon that adsorbs carbon tetrachloride upstream of the check valves before the soil vapor is vented to the atmosphere. The check valve prohibits flow of atmospheric air into the borehole during a reverse barometric pressure gradient, which tends to dilute and spread carbon tetrachloride vapors in the subsurface.

The wells are sampled periodically upstream of the granular activated carbon canisters. During FY 2009, the maximum carbon tetrachloride concentrations ranged from 10 to 17 ppmv at the four wells (299-W18-6, 299-W18-7, 299-W18-246, and 299-W18-252) near the 216-Z-1A Tile Field. The maximum carbon tetrachloride concentrations ranged from 5 to 12 ppmv at the four wells (299-W18-10, 299-W18-11, 299-W18-12, and 299-W18-247) near the 216-Z-18 Crib.

10.2 Tank Farm Activities

D. A. Myers, H. A. Sydnor, J. G. Field, and D. L. Parker

The Vadose Zone Integration Program is responsible for implementing the tank farm *Resource Conservation and Recovery Act of 1976* corrective action program through field characterization, laboratory analyses, technical analyses, risk assessment for past tank leaks, and installation of interim measures to reduce the threat from contaminants until permanent solutions can be found. In CY 2009, direct-push boreholes were installed for soil sampling and geophysical logging in the C and TY Tank Farms (Section 10.2.1). Surface geophysical exploration at WMA S-SX was completed (Section 10.2.2). Section 10.2.3 provides a brief discussion on geophysical logging results. Section 10.2.4 describes the interim surface barrier work associated with the TY Tank Farm to reduce infiltration of precipitation.

10.2.1 Direct-Push Boreholes and Sampling

A hydraulic hammer unit was deployed in three tank farms during the reporting period to evaluate subsurface contamination in the vadose zone. Pushes were made at five sites in the C Tank Farm to investigate past releases in and adjacent to the tank farm. The hydraulic hammer unit was deployed at thirteen sites in the SX Tank Farm to assess the extent of contamination in support of a proposed interim barrier. The sites were identified based on previous investigations of subsurface resistivity (RPP-RPT-42513, *Surface Geophysical Exploration of the SX Tank Farm at the Hanford Site*). Table 10-2 lists the locations where direct push was used in the single-shell tank farms. The table also indicates the purpose of the probe holes and the number of electrodes installed in each hole. The hydraulic hammer unit was deployed at fifteen sites in the TY Tank Farm in support of a proposed interim barrier over that facility. The sites investigated were previously identified using subsurface resistivity (RPP-RPT-38320, *Surface Geophysical Exploration of the TX and TY Tank Farms at the Hanford Site*).

A multi-level sampler was used at most sites to collect samples of potentially contaminated sediments for laboratory analysis. In addition, the hydraulic hammer unit was used to place deeply buried electrodes at each of the investigated sites.

In 2009, the first installation of a multiple-depth electrode string was made in the C Tank Farm. These electrodes will be used during a future deployment of surface geophysical exploration in the tank farms. The analytical results will be used to support placement of a proposed interim barrier over all or part of the SX Tank Farm, an interim barrier of the TY Tank Farm, and the Phase 2 (tank farm closure) investigation of the C Tank Farm.

10.2.2 Surface Geophysical Exploration

Surface geophysical exploration (a combination of surface-deployed geophysical techniques) was applied at WMA S-SX during the reporting period (RPP-RPT-42513). The primary tool applied through surface geophysical exploration is pole-pole electrical resistivity. Other tools applied during FY 2008 at this site include electromagnetic induction, magnetic gradiometry, and ground-penetrating radar, which are used to help define the presence and distribution of buried infrastructure so those features can be considered during the resistivity data analysis. The depth to which the resistivity measurements interrogate the subsurface is determined by the distance between electrode pairs (i.e., the further apart, the deeper the interrogation). Because resistivity is an indirect measure of several subsurface phenomena (e.g., moisture distribution, saline contaminants, and soil texture), the further the separation between the electrode pairs, the lower the resolution of the analysis. The resistivity data are mathematically analyzed through a process known as inversion to provide a best estimate of the distribution of resistivity anomalies. Surface geophysical exploration provides a means of extrapolating direct measurements taken by sampling, logging, or other means to provide a cost-effective overview of large areas that may have been impacted by a variety of waste management practices.

In WMA S-SX, the surface geophysical exploration analytical results will assist in the design of an interim surface barrier, including definition of areas that will be confirmed using direct-push sampling (RPP-RPT-42513). Figure 10-2 provides a plan view and an isometric, composite view of the WMA. The figure also shows areas of high conductance (low resistivity) in the vadose zone. These areas likely correspond to areas of high concentration of nitrate and associated contaminants.

Analysis of the first-ever, fully three-dimensional (including buried electrodes) surface geophysical exploration survey was completed during the reporting period. The survey covered an unplanned release site associated with the CR-151 diversion box (RPP-RPT-41236, *Surface Geophysical Exploration of UPR 200-E-81 Near the C Tank Farm*). In the survey, 233 electrodes were placed over the area of the known release, including four electrodes placed in two direct-push holes. The entire array was then interrogated both forward and reciprocally. The results of this survey are shown in Figure 10-3, which presents an isometric view of the interpreted results.

10.2.3 Geophysical Logging

Geophysical logging of selected dry wells in the T Tank Farm was conducted to support assessment of the interim surface barrier placed over the site of the 1973 release from tank 241-T-106.

Geophysical logging of direct-push boreholes was also performed. During CY 2009, the slim-hole capability was enhanced by deploying a bismuth-germanate tool that provides spectral-gamma capability. In addition to the bismuth-germanate logs, a neutron moisture log was run at each investigative site. These logs are used to select specific sampling intervals.

10.2.4 Interim Barrier

In 1973, tank 241-T-106 leaked ~435,000 liters of waste into the surrounding soil (RPP-23752, *Field Investigation Report for Waste Management Areas T and TX-TY*). Contamination from this leak is present in the vadose zone beneath the T Tank Farm. The T Tank Farm interim surface barrier was installed to reduce the infiltration of water into the area of contamination (i.e., decrease the potential for further contaminant migration) and to serve as a barrier demonstration project. Construction of the T Tank Farm interim surface barrier was completed in March 2008. The barrier is ~6,575 square meters and consists of ~0.6 to 0.9 meters of engineered fill covered by a geotextile and a spray-applied polyurea/polyurethane (RPP-ENV-33430, *RPP NEPA Screening Form and Categorical Exclusion for the 241-T-106 Interim Infiltration Barrier*).

The effectiveness of the T Tank Farm interim surface barrier to reduce vadose zone moisture is being assessed through a barrier monitoring program (PNNL-16538, *T Tank Farm Interim Surface Barrier Demonstration – Vadose Zone Monitoring*). A solar-powered and remotely controlled system was installed to monitor soil-water conditions continuously at four locations beneath the barrier and outside the barrier footprint, as well as site meteorological conditions. Each location has a capacitance probe with multiple sensors, multiple heat-dissipation units, and a neutron probe access tube. The principal variables monitored are soil water content and soil water pressure. Soil temperature, precipitation, and air temperature are also measured. The *T Tank Farm Interim Surface Barrier Demonstration – Vadose Zone Monitoring FY07 Report* (PNNL-17306) reports pre-barrier data, and a future monitoring report will provide post-barrier data.

An effort is currently underway to construct an interim surface barrier over the TY Tank Farm. The new barrier will differ from the T-106 interim barrier in several ways:

- All of the tanks will be covered.
- The barrier will consist of modified asphalt.
- Runoff will be directed to an evapotranspiration basin where it will be redirected back to the atmosphere.

The design for the new interim surface barrier has been completed, and construction contracts are scheduled to be released in early 2010.

10.3 Upscaled Flow Properties for Heterogeneous Hanford Sediments

R. Khaleel and Z. F. Zhang

Hanford sediments are inherently heterogeneous at a variety of scales. A conventional approach to modeling flow in such media is to incorporate into models the overall heterogeneity of the system. However, because of spatial variability in hydraulic properties, it is inappropriate to use measurements from a few small-scale laboratory experiments to model the large, field-scale behavior. An alternative approach is to define an equivalent homogeneous medium with effective or macroscopic flow properties and thereby predict the mean flow behavior at the field scale. To represent a heterogeneous medium by its homogeneous equivalent, however, the upscaled or effective flow properties representing the equivalent homogeneous

medium need to be estimated. Thus, upscaling uses the local (Darcy) scale laboratory (core) measurements to represent unsaturated flow at the field scale.

During FY 2009, work was completed on the development and application of an upscaling approach for hydraulic properties. The objective of this section is to present a summary of the upscaling methodology and its application for Hanford sediments. In "Describing the Unsaturated Hydraulic Properties of Anisotropic Soils Using a Tensorial Connectivity-Tortuosity (TCT) Concept" (Zhang et al. 2003), a tensorial connectivity-tortuosity (TCT) model was proposed to describe directional unsaturated hydraulic conductivity. The TCT model is combined with a power-averaging model ("Random Porous Media Flow on Large 3-D Grids: Numerics, Performance, and Application to Homogenization" [Ababou 1996]) to describe the macroscopic unsaturated hydraulic conductivity for field soils. Numerical simulations were conducted using the Subsurface Transport Over Multiple Phases (STOMP) flow simulator (PNNL-15782, *STOMP Subsurface Transport Over Multiple Phases Version 4.0 User's Guide*); details are described in "Simulating Field-Scale Moisture Flow Using a Combined Power-Averaging and Tensorial Connectivity-Tortuosity Approach" (Zhang and Khaleel 2010). The numerical results are compared with moisture content profiles for a field injection experiment at the Sisson and Lu site, which is located in the 200 East Area south of the Plutonium-Uranium Extraction (PUREX) Plant.

The field injection site was specifically designed by Sisson and Lu (RHO-ST-46P, *Field Calibration of Computer Models for Application to Buried Liquid Discharges: A Status Report*) to understand moisture movement underneath buried discharges, such as tank leaks. The Sisson and Lu site was used for a field infiltration experiment from June to July 2000 (PNNL-13679, *Vadose Zone Transport Field Study: Status Report*; PNNL-13795, *Vadose Zone Transport Field Study: Soil Water Content Distributions by Neutron Moderation*). Initial moisture content distribution was measured on May 5, 2000, at the 32 radially and symmetrically arranged cased boreholes (Figure 10-4a). Injections began on June 1 (the 153rd day of the year), and 4,000 liters of water were metered into an injection point 5 meters below the land surface over 6 hours. Similarly, 4,000 liters of water were injected in each subsequent injection on June 8, June 15, June 22, and June 28. During the injection period, neutron logging in 32 wells took place within a day (i.e., June 2, June 9, June 16, and June 23) following each of the first four injections. A wildfire near the field site prevented immediate logging of the moisture content (θ) distribution for the fifth injection on June 28. Three additional readings of the 32 wells were subsequently completed on July 7, July 17, and July 31. During each neutron-logging event, moisture content was recorded in each well at a depth interval of 0.3048 meters, starting from a depth of 3.9625 meters and continuing to a depth of 16.764 meters, resulting in a total of 1,376 measurements in each of the eight observation days over a 2-month period. Because of the unique three-dimensional nature of the database and its importance in understanding transient moisture movement from a point-source leak in an arid setting in imperfectly stratified heterogeneous unsaturated media, the 2000 Sisson and Lu field data have been the subject of a variety of recent modeling efforts, such as the following:

- "Estimation of Effective Unsaturated Hydraulic Conductivity Tensor Using Spatial Moments of Observed Moisture Plume" (Yeh et al. 2005)
- "Upscaling Unsaturated Hydraulic Parameters for Flow through Heterogeneous Anisotropic Sediments" (Ward et al. 2006)

- "Simulation of Field Injection Experiments in Heterogeneous Unsaturated Media using Cokriging and Artificial Neural Network" (Ye et al. 2007)
- "A Markov Chain Model for Characterizing Medium Heterogeneity and Sediment Layering Structure" (Ye and Khaleel 2008)
- "Quantification of Uncertainty in Pedotransfer Function-Based Parameter Estimation for Unsaturated Flow Modeling" (Deng et al. 2009).

The dominance of lateral movement is a unique feature of unsaturated flow, especially in an arid setting. Horizontal stratification in geologic strata such as that found in the 200 Areas Central Plateau enhances such movement because, at high tension (i.e., dry soil), hydraulic conductivities of fine-textured materials are relatively high, and the fluid prefers to spread laterally in the fine media rather than to move vertically into the underlying coarse media. The effects of textural heterogeneities on moisture movement are further enhanced by the variability in θ, a phenomenon referred to as moisture-dependent anisotropy ("Stochastic Analysis of Unsaturated Flow in Heterogeneous Soils 2. Statistically Anisotropic Media with Variable α" [Yeh et al. 1985]) and shown to be a dominant mechanism for lateral flow at the Sisson and Lu site ("Stochastic Analysis of Moisture Plume Dynamics of a Field Injection Experiment" [Ye et al. 2005]).

The water content data points from the 32 observation wells during each observation were interpolated onto a three-dimensional grid. Figure 10-5 shows the observed water content differences after subtracting the initial θ from the measured θ for the six different dates. (Note that for easy viewing of the plume shape and size, water content increases less than 0.005 $m^3\ m^{-3}$ were blanked out.) In total, ~54% of the injected water had moved out of the monitored region 33 days (213th day of the year) after the last injection. Almost no injected water migrated below the ~12-meter depth, which suggests that the relatively finer Unit E underlain by a coarser Unit F behaved like a capillary barrier to prevent moisture from moving into Unit F (Figure 10-5).

To apply the power-averaging TCT model, the hydraulic properties at the core scale were derived from two sources: *Laboratory Measurements of the Unsaturated Hydraulic Properties at the Vadose Zone Transport Field Study Site* (PNNL-14284) and "Evaluation of van Genuchten-Mualem Relationships to Estimate Unsaturated Conductivity at Low Water Contents" (Khaleel et al. 1995). Power averaging provides the directional effective unsaturated hydraulic conductivity at discrete values of pressure head, h (Zhang and Khaleel 2010). Note that the power-averaging factor, p, can take any value between -1 and 1. The effective unsaturated hydraulic conductivity, $K^e(h)$, for each stratum was determined with different combinations of (p_1, p_2, p_3) in the (x, y, z) directions, where z is aligned with the vertical direction. The effective tortuosity-connectivity coefficients L^e ("A New Model for Predicting the Hydraulic Conductivity of Unsaturated Porous Media" [Mualem 1976]) were obtained for each anisotropic equivalent homogeneous medium via the TCT model using a least-square fit for the effective K^e versus h data pairs.

The degree of macroscopic anisotropy in hydraulic conductivity at the field site is not known a priori, except that horizontal stratification was visually observed in each of the stratigraphic units. For comparison purposes, the results are reported for four typical cases representing isotropy (ISO), low anisotropy (LA), intermediate anisotropy (IA), and high anisotropy (HA) (Table 10-3). For the Sisson and Lu site, the simulation results best matched the observations when the power values of 1 and one-third were used for determining the $K^e(h)$ in the horizontal and vertical

directions, respectively. These power values suggest a rather mild, macroscopic anisotropy for the field site.

To quantitatively evaluate the combined power-averaging TCT model, the temporal evolution of spatial moments is used to quantify the center of mass and the spread of the injected water for the observed and simulated moisture plumes (Zhang and Khaleel 2010). Figure 10-6 compares the total injected water volume with the volume retained in the region of observation. For all cases, the estimation matched the observation reasonably well before the third injection. Beyond the third injection, the isotropic case over-estimated the total volume, while the two cases with intermediate anisotropy and high anisotropy under-estimated the total volume. The case with low anisotropy predicted the total water volume the best. Note that the numerical error in mass balance over the entire simulation domain was no more than 0.16% for all cases.

As with the Sisson and Lu site, the lateral moisture movement was predominantly southeastern (Ye at al. 2005); however, the fluid volume that migrated out of the monitored region could not be considered in the moment analysis because its specific locations were unknown. Consequently, the center of mass in the *x* and *y* directions from the moment analysis for both observed and simulated plumes showed little variation with time (not shown here). The simulation of low anisotropy gives the best fit for mass center in the vertical (*z*) direction. Figure 10-7 shows the observed and simulated centers of the injected fluid plume within the monitored region in the *z* direction. Again, low anisotropy gave the best prediction, while isotropy over-estimated, and intermediate anisotropy and high anisotropy under-estimated the movement in the vertical direction. Unlike other cases, the trend in the movement of mass center in the *z* direction for low anisotropy and the observed plumes is similar, and the comparison between the two is reasonably good. As both low anisotropy and the observed plumes indicate, the mass centers moved most rapidly during the early part of the injection experiment. In the *z* direction, the mass center for the observed plume traveled downward ~1 meter for the first 15 days but ~1.1 meter in the following 45 days (Ye et al. 2005).

Figure 10-8 illustrates the temporal evolution of components of the spatial variance tensor as an indication of the spreading of the injected water. The observed spatial variances (σ^2_{xx}, σ^2_{yy} and σ^2_{zz}) of the plume increased with time, indicative of the continuous spreading of the plume around its mass center in the *x*-, *y*-, and *z*-directions during the injection experiment. The larger spatial variances in the *x*- and *y*-directions than in the *z*-direction suggest a greater spreading in the horizontal plane than in the vertical. The cross-covariances (σ^2_{xy}, σ^2_{xz} and σ^2_{yz}) are non-zero because the principal directions of the moisture plume were not aligned with the *x*-*y*-*z* coordinate system. Among all cases, the simulation of low anisotropy predicted the spreading the best. The isotropic case over-estimated, whereas intermediate anisotropy and high anisotropy under-estimated the vertical spreading. The opposite is true for the lateral spreading. Note the considerable deviation of high anisotropy- and intermediate anisotropy-based spatial variances, compared to the observed spatial variances. However, unlike other cases, the trend in the magnitude of spreading (Figure 10-8) for different days for the observed plume and low anisotropy is similar; the low anisotropy-based variance matches best the observed variance during injection as well as during redistribution of the moisture.

To quantify the error for the observed versus simulated plume, the absolute values of the percent errors for seven observation dates are illustrated in

Table 10-4. Among all the simulation cases, low anisotropy had the smallest error (between 5.5% and 9.8%) and intermediate anisotropy had the second smallest error (between 14.3% and 53.3%), while high anisotropy and isotropy had the largest error (between 17.3% and 80.7%).

While not known a priori, it is expected that the degree of macroscopic anisotropy at a field site is somewhere in between the extremes of isotropic and perfectly stratified media. As shown, the combined power-average and TCT model has the flexibility to determine directional effective unsaturated hydraulic conductivity having differing degrees of anisotropy. The combined power-averaging TCT model can thus describe the macroscopic anisotropy of any degree. However, the power values used in the power averaging are not unique; it is also possible to optimize for the power values via an inverse procedure.

At the Sisson and Lu site, based on the spatial pattern of simulated and observed moisture plumes during infiltration and redistribution, the anisotropy of the flow field, even though mild for the low tension of 1 meter, appears to be tension- or moisture-dependent with a more pronounced lateral spreading at the edges of the moisture plume (marginally wet) than inside the core of the plume (wet). This is consistent with the findings of Yeh et al. (1985) and "Effective Hydraulic Conductivities of Transient Unsaturated Flow in Stratified Soils" (Mantoglou and Gelhar 1987) for the moisture-dependent anisotropy of the effective conductivity for unsaturated flow.

Note that a variety of other approaches were used here to simulate the Sisson and Lu field injection experiment (Yeh et al. 2005; Ward et al. 2006; Ye et al. 2007; Ye and Khaleel 2008; Deng et al. 2009). However, the preceding models need initial soil water content distribution and/or snapshots of moisture content distribution during a transient field experiment. These data are typically not available for most field sites. Unlike the above methods, the combined power-average and TCT model is based on the measured hydraulic properties for small core samples and, hence, has a more general applicability.

In summary, a practical approach based on combined power averaging and a TCT concept was used to estimate the effective unsaturated hydraulic conductivity tensor for equivalent homogeneous media. Power averaging provides the directional effective unsaturated hydraulic conductivity at discrete pressure head, h, values. The effective tortuosity-connectivity coefficients L^e were obtained for each anisotropic equivalent homogeneous medium via the TCT model using a least-square fit for the effective K^e versus h data pairs. It was found that, for the Sisson and Lu field injection site, the simulation results match the observations the best when the power values of 1 and one-third were used for determining the $K^e(h)$ in the horizontal and vertical directions, respectively. These power values suggest a rather mild, macroscopic anisotropy for the field site. The spatial moments of the simulated moisture plume based on the effective hydraulic conductivities are in good agreement with those for the observed plume. The macroscopic anisotropy does indeed vary with decreasing moisture content. At this particular field site, the power-averaging and TCT-based effective hydraulic properties of an equivalent homogeneous medium yield a similar temporal evolution of spatial moment of the observed moisture plume.

Table 10-1. Carbon Tetrachloride Inventory Removed by Vapor Extraction from Primary Disposal Sites.

Well Field	Mass Removed Using Soil Vapor Extraction, April 2009 to September 2009 (kg)	Mass Removed Using Soil Vapor Extraction, 1991 to September 2009 (kg)
216-Z-1A	73*	24,845*
216-Z-18		
216-Z-9	103	54,711
Totals	**177***	**79,557***

Notes:
* Total due to rounding.

Table 10-2. Direct-Push Holes Investigations Summary Table.

Tank Farm, Purpose	Investigative Sites	Number of Site Soil Samples Collected	Total Number of Samples	Slim Hole Logging Performed
TY Tank Farm, barrier investigation	15	11	28	Spectral gamma,moisture
SX Tank Farm, barrier investigation	13	11	36	Spectral gamma,moisture
C Tank Farm, Phase 2	5	5	39	Spectral gamma,moisture

Table 10-3. Numerical Simulation Cases with Varying Anistropy.

Case	Anisotropy Level	*p* Value for Horizontal Direction (*i* = 1, 2)	*p* Value for Vertical Direction (*i* = 3)
ISO	Isotropy	0	0
LA	Low anisotropy	1	⅓
IA	Intermediate anisotropy	1	0
HA	High anisotropy	1	-1

Notes:
* This table is based on "Simulating Field-Scale Moisture Flow Using a Combined Power- Averaging and Tensorial Connectivity-Tortuosity Approach" (Zhang and Khaleel 2010).
HA = high anisotropy
IA = intermediate anisotropy
ISO = isotropy
LA = low anisotropy

Table 10-4. Computed Mean Error (%) for the Observed Versus Simulated Plume for Different Simulation Cases.

Criterion	Case			
	ISO	LA	IA	HA
Mass	48.1	6.3	14.9	22.1
z_c	17.3	7.6	20.6	27.7
σ_{xx}^2	40.1	7.5	18.0	25.4
σ_{yy}^2	41.4	5.5	14.3	22.6
σ_{zz}^2	44.4	9.8	53.3	80.7

Notes:
* This table is based on "Simulating Field-Scale Moisture Flow Using a Combined Power- Averaging and Tensorial Connectivity-Tortuosity Approach" (Zhang and Khaleel 2010).
HA = high anisotropy
IA = intermediate anisotropy
ISO = isotropy
LA = low anisotropy

Figure 10-1. Locations of Carbon Tetrachloride Soil Vapor Extraction Wells at 216-Z-1A/216-Z-12/216-Z-18 and 216-Z-9 Well Fields.

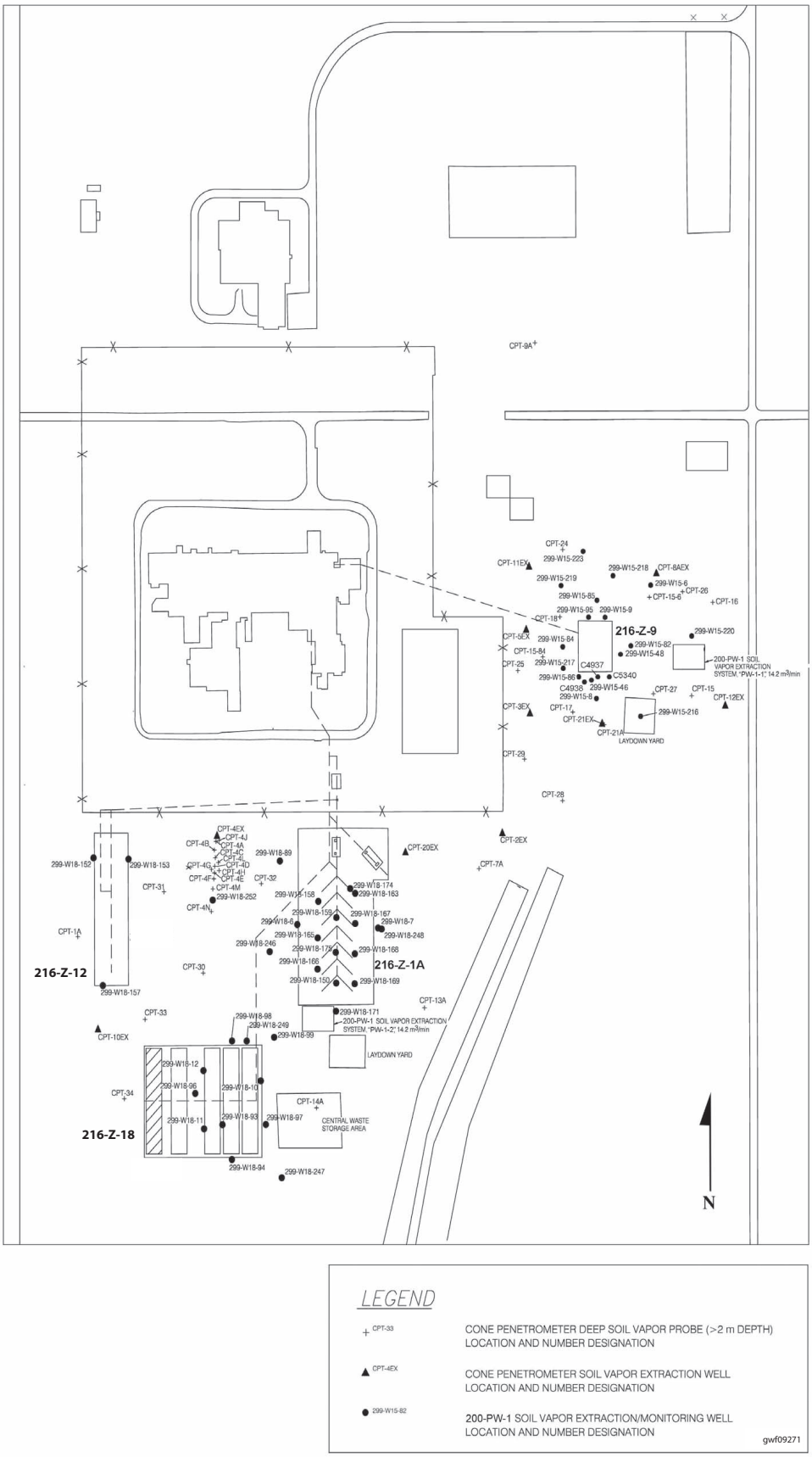

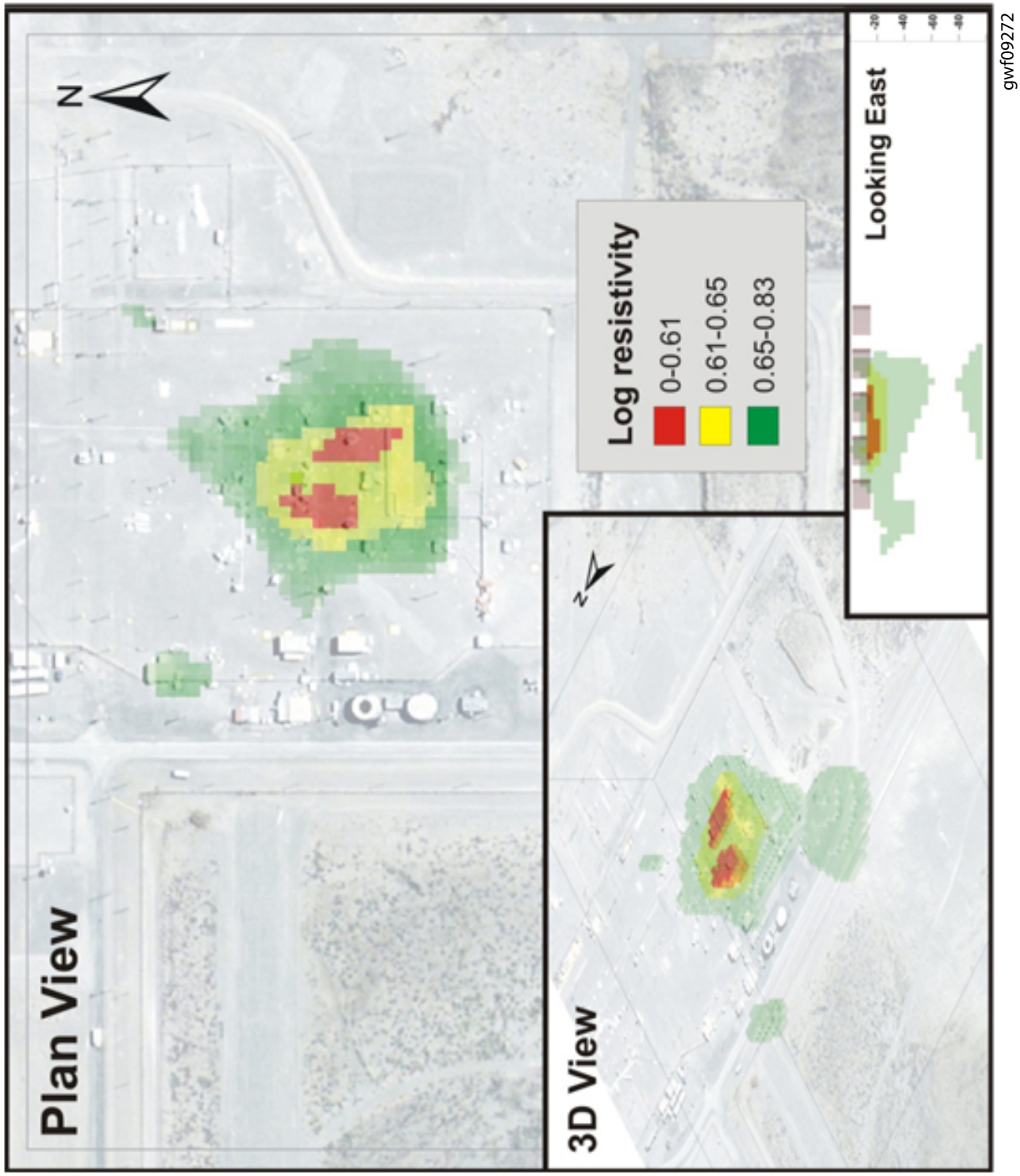

Figure 10-2. Results Showing Views for Selected Resistivity Levels, Waste Management Area S-SX.

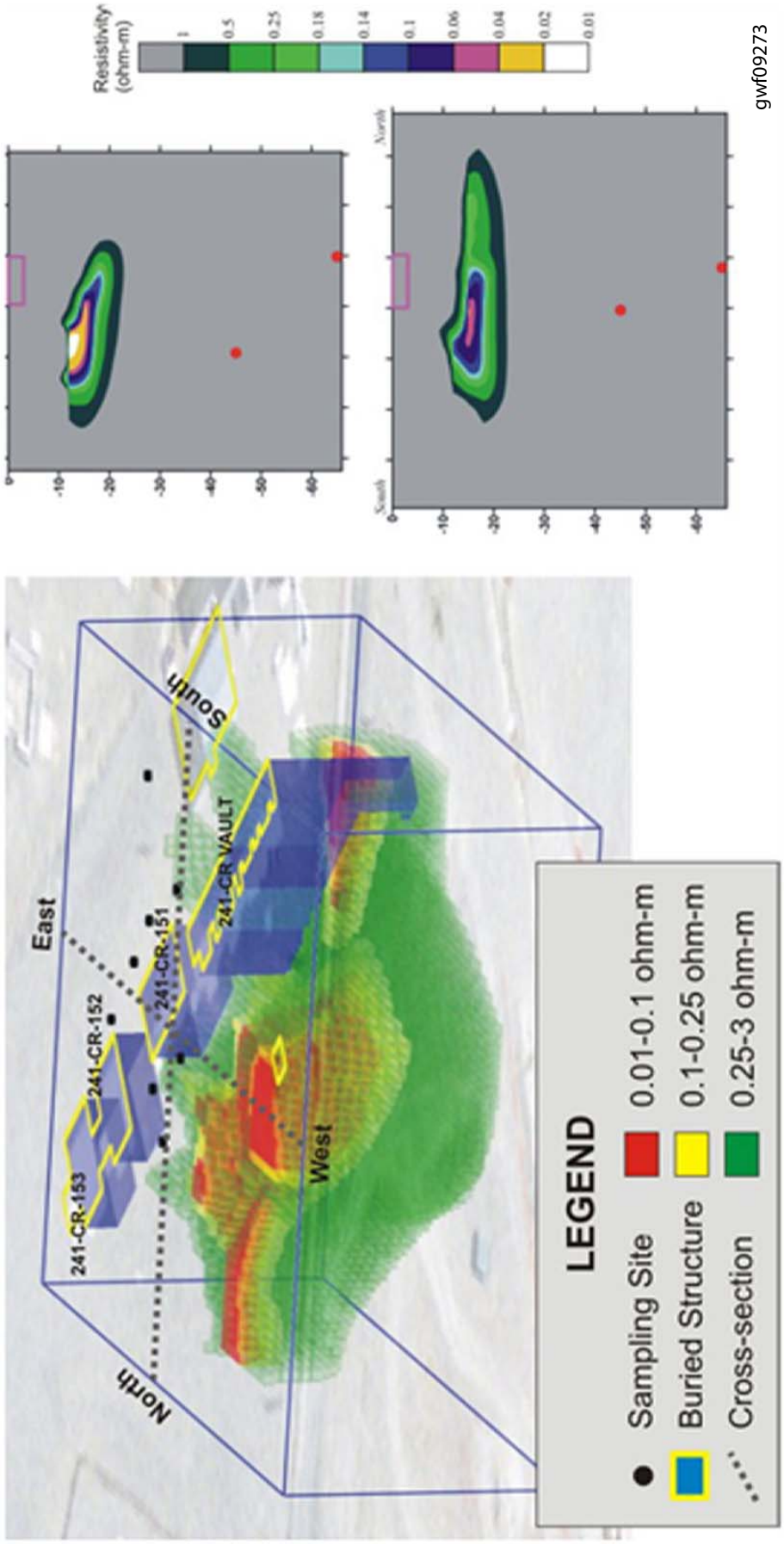

Figure 10-3. Isometric View of UPR-200-E-81, Fully Three-Dimensional Surface Geophysical Exploration.

Figure 10-4. (a) Plan View of the Layout of the 200 Injection Well (Empty Circle near the Center, the Sampling Boreholes (Empty Squares), and the Observation Wells (Filled Circles) at the Sisson and Lu Site and (b) the A-A' Cross-Section Showing the Lithostratigrapy (Modified After PNNL-13631, Sampling of Boreholes WL-3A through -12 in Support of the Vadose Zone Transport Field Study). Plot (b) Also Shows the Sample Locations and the Percentage of Fine Particles (After Zhang and Khaleel 2010). Measured Moisture Content (MC) Differences Showing the Moisture Plume for D.

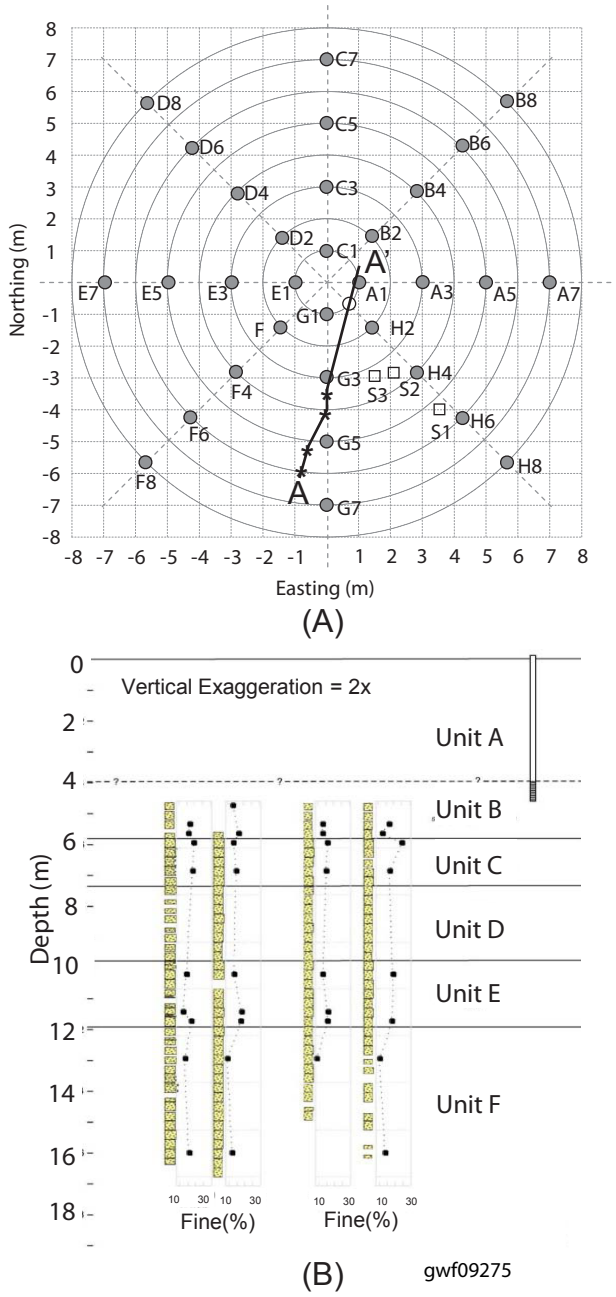

Figure 10-5. Measured Moisture Content (MC) Differences Showing the Moisture Plume for Different Days. Five Weekly Injections Took Place Between June 1 (DOY 153) and June 28 (DOY 180) 2000. The Letters B through F Denote the Five Stratigraphic Units (After Zhang and Khaleel 2010).

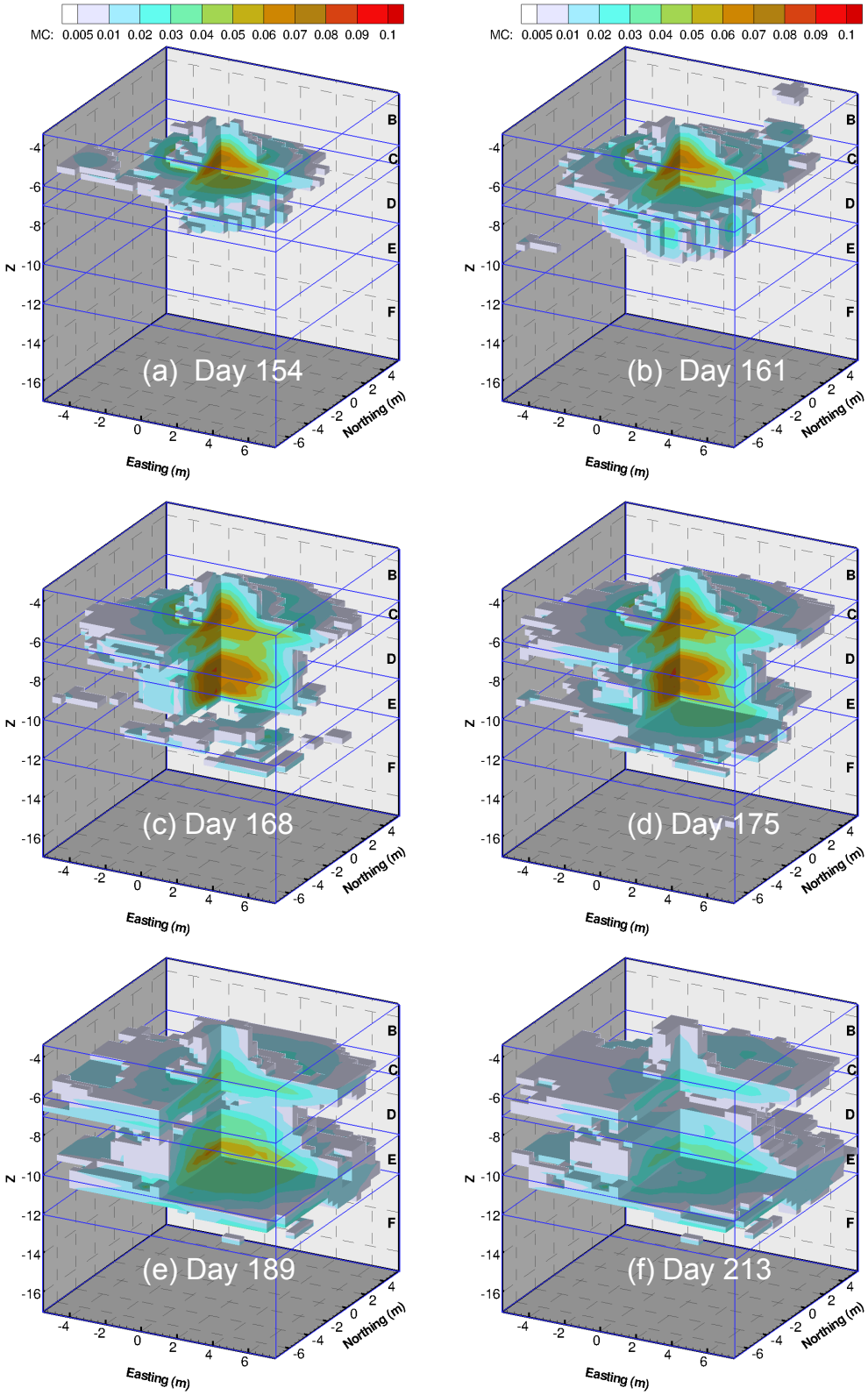

gwf09276

Figure 10-6. Comparison of Injected Water Volume and Water Volume Retained in the Region of Observation (After Zhang and Khaleel 2010).

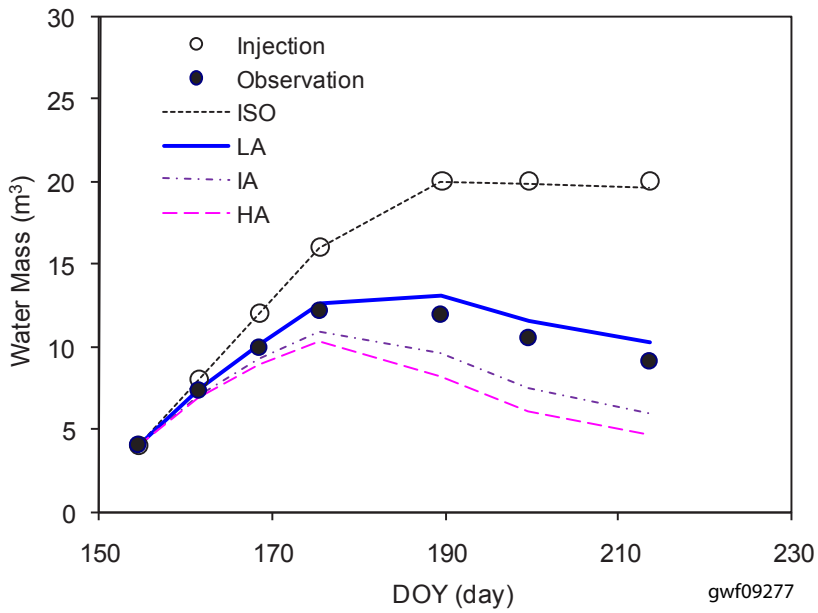

ISO= Isotropic, LA = Low Anisotropy, IA = Intermediate Anisotropy, HA = High Anisotropy

Figure 10-7. The Observed and Simulated Center of Mass in the z (Vertical) Direction (After Zhang and Khaleel 2010).

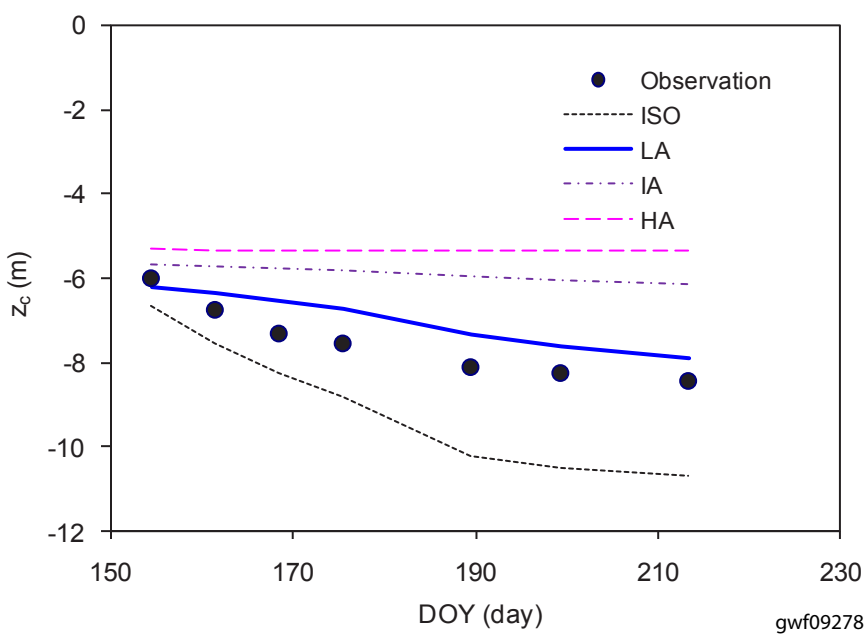

ISO= Isotropic, LA = Low Anisotropy, IA = Intermediate Anisotropy, HA = High Anisotropy

Figure 10-8. The Spreading of the Moisture Plume in the a) x (Easting), b) y (Northing), and c) z (Vertical) Directions Based on the Diagonal Components of the Second Moments (After Zhang and Khaleel 2010).

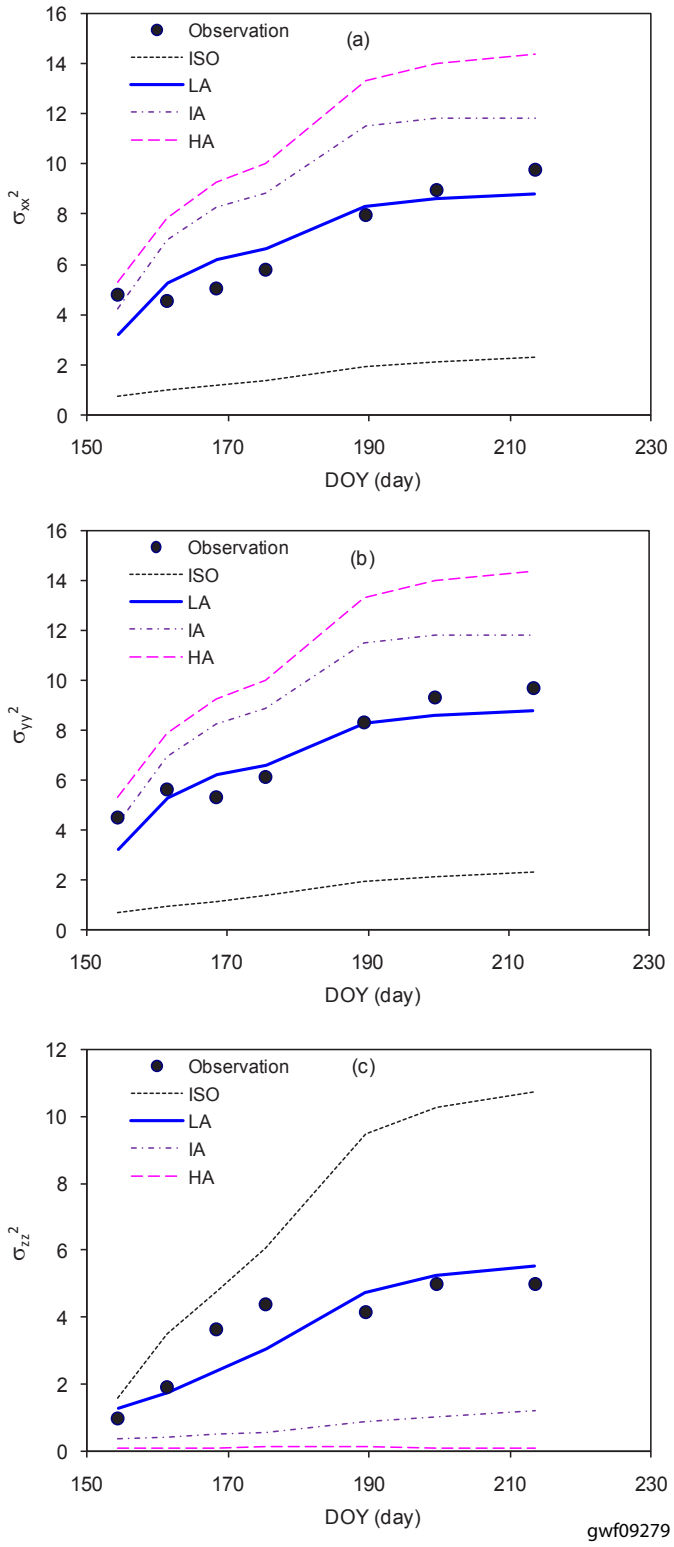

ISO= Isotropic, LA = Low Anisotropy, IA = Intermediate Anisotropy, HA = High Anisotropy